Appl Phys A (2012) 109:291–297
DOI 10.1007/s00339-012-7044-x

Applied Physics A
Materials Science & Processing

Ti:sapphire femtosecond laser direct micro-cutting and profiling of graphene

W. Zhang · L. Li · Z.B. Wang · A.A. Pena · D.J. Whitehead · M.L. Zhong · Z. Lin · H.W. Zhu

Received: 8 May 2012 / Accepted: 27 June 2012 / Published online: 19 July 2012

Abstract This paper reports the formation of uniform single layer micro-patterns of graphene on a glass substrate using direct femtosecond laser cutting. The cutting of graphene was achieved in air and argon. By translating the graphene sample with respect to the laser beam, continuous micro-channels were carved. The cutting geometry can be controlled by varying the laser fluence and the scanning path. Also, 1∼2 μm wide graphene micro-ribbons were hatched out. The ablation threshold of graphene was determined to be 0.16∼0.21 J/cm^2. With the laser fluence higher than the ablation threshold, graphene was ablated rapidly and removed completely without damaging the glass substrate. Atomic force microscopy (AFM) and Raman spectroscopy have been used to confirm the ablation of graphene. Time domain finite difference modelling was employed to understand the thermal history of the laser ablation process.

1 Introduction

Graphene, a recently discovered material, is a flat monolayer of carbon atoms arranged in a honeycomb lattice [1–3]. The research on graphene has continued into both large-area synthesis of graphene films, and understanding its unusual properties including ultra-high carrier mobilities [4], and superb thermal conduction property at room temperature (∼5000 W/m/K) [5]. In particular, the electronic properties of graphene are of great interest and are also among the most explored aspects [4]. So far, the fabrication of wafer-scale graphene sheets has been demonstrated using the standard chemical vapour deposition (CVD) method [6], which holds unique advantages of high quality and low cost. At present, a challenge is the selective patterning of graphene for certain electronic applications (e.g. graphene-based micro/nano-scale devices). Although patterning of graphene can be achieved using recently developed methods such as O_2 plasma etching in combination with a mask [7], laser shock nano-punching of graphene that is placed on a pre-patterned substrate [8], or spatially controlled epitaxial graphene synthesis using pulsed excimer laser irradiation, which is based on surface decomposition of SiC [9], a technique toward low-cost, high-throughput, and maskless production of graphene devices is still under development.

Ultra-fast pulse lasers (pulse duration $<$ 100 ps) have been demonstrated to be a promising tool for micro-processing of a variety of materials with low heat affected zones in the surrounding materials [10]. So far, very few experiments on ultra-fast laser direct ablation of graphene have been described. Currie et al. studied the femtosecond laser induced damages on graphene and has shown that even at a very low laser fluence of 14 mJ/cm^2, some modifications of graphene lattice can be observed [11]. Roberts et al. studied 50 fs laser pulse interaction with graphene and has demonstrated a clean micro-hole formed on graphene by a single pulse laser shot [12]. Several other techniques including femtosecond laser direct-writing of 40 nm thick graphene films [13] and graphene oxides films [14, 15] have been proposed. However, laser fabrication of complex micro-patterns on single layer graphene has not been reported. This paper reports a femtosecond laser direct patterning technique by design-

W. Zhang (✉) · L. Li · Z.B. Wang · A.A. Pena · D.J. Whitehead
Laser Processing Research Centre (LPRC),
School of Mechanical, Aerospace and Civil Engineering,
The University of Manchester, Manchester M13 9PL, UK
e-mail: wen.zhang-2@postgrad.manchester.ac.uk

M.L. Zhong · Z. Lin · H.W. Zhu
Department of Mechanical Engineering, Tsinghua University,
Beijing 100084, China

ing the laser scanning path, and demonstrates high quality laser cutting of micro-channels and micro-ribbons on single layer CVD graphene at room temperature. The effects of laser cutting of graphene in air and in Argon atmosphere have been compared. By taking advantage of the ultra-short femtosecond laser pulses, precise cutting of graphene with well-defined and clean edges has been achieved. This technique will open up opportunities of micro/nano-processing of graphene in a fast, low-cost, and reproducible manner.

2 Experimental procedure

The graphene samples used in this work were grown on copper foils by CVD method similar to that described in [6]. After the growth, the copper substrate was dissolved by a mixed $FeCl_3$ and HCl solution. The graphene films were separated (floating on top of the solution) and then they were rinsed by de-ionized water, and finally transferred to thin borosilicate glass substrates. Transferred graphene films are found flat and optically uniform on the glass substrate in spite of minor flaws, i.e. folds or cracks. The thickness of pristine graphene is clearly identified to be predominantly single-layer by Raman spectrometer, according to a method described by Ferrari et al. [16]. Figure 1 shows the Raman spectrum of the pristine graphene, which demonstrates typical features of monolayer graphene: a sharp symmetric 2D peak centered at 2690 cm^{-1} with a full width at half maximum (FWHM) of ~35 cm^{-1}, and a ~0.3 I_G to I_{2D} ratio. This clearly indicates the single layer graphene structure [6, 16]. The D band indicates few defects.

A Ti:sapphire laser (Coherent Libra) with a central wavelength of 800 nm, TEM_{00} beam mode and a pulse duration of 100 fs was used in this research. The output repetition rate was fixed to 1 kHz. The laser pulse energy was varied via the use of a neutral-density filter attenuator. A 15× objective lens (Edmund) with a numerical aperture (NA) of 0.28 and a focal length of 13.3 mm was used to focus the laser beam. Laser power was measured after the focusing lens. A three-axis stage (Aerotech) was employed to translate the graphene sample perpendicular to the laser beam. The experimental setup of femtosecond laser ablation is shown in Fig. 2.

Laser processing of graphene was carried out at room temperature (RT) in air and in the presence of Argon gas, respectively. In the case of Argon environment, a sealed box with a piece of glass lid was utilized to contain graphene sample (Fig. 2b). The glass was chosen to be transparent at 800 nm wavelength. During the laser processing, Argon gas was supplied to the box all the time through an inlet, so the

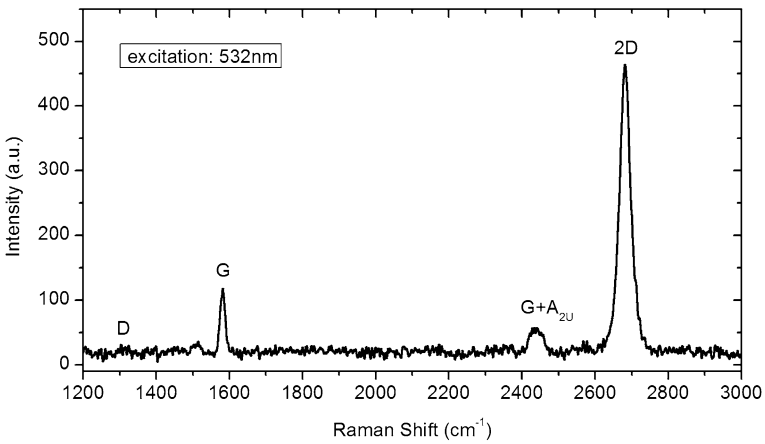

Fig. 1 Raman spectrum of pristine graphene on glass with baseline correction. The measurements were performed with a light source of 532 nm CW laser and a 50× objective lens at room temperature. The spectrum was acquired over a range from 1200 to 3000 cm^{-1} with the excitation laser power of ~2 mW to avoid laser-induced heating

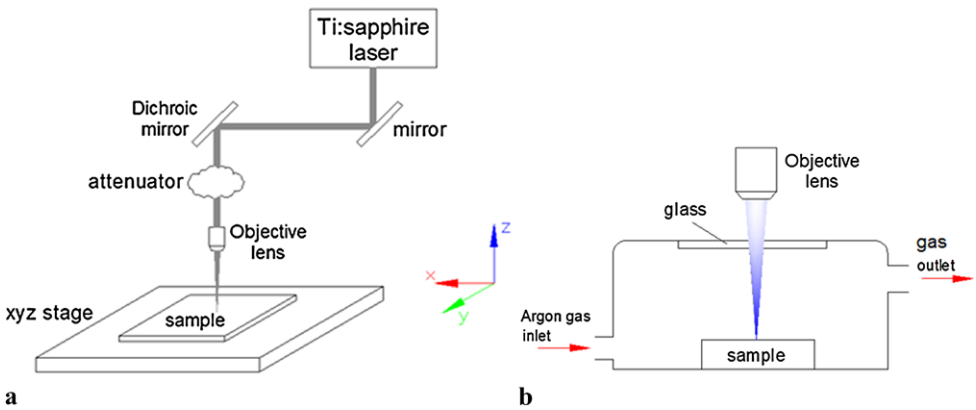

Fig. 2 Schematic diagram of experimental setup of the femtosecond laser ablation system (**a**) in air and (**b**) in Argon atmosphere

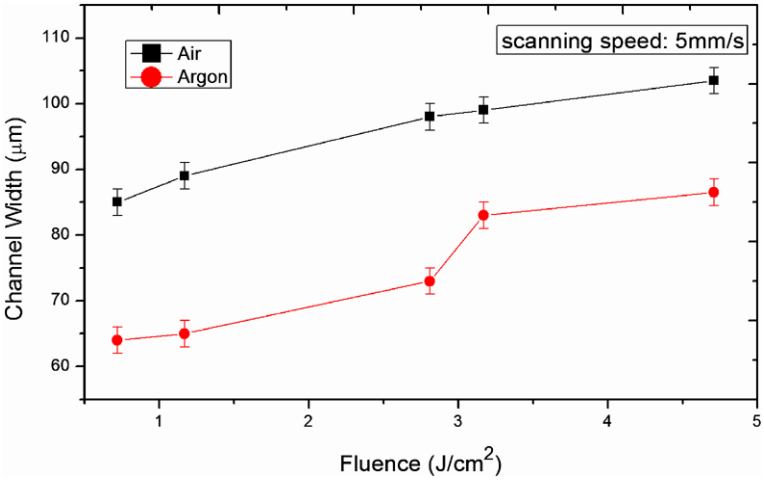

Fig. 3 Widths of the channels cut in air (*black line*) and in argon (*red line*) with the same processing parameters

air/oxygen could be expelled from the outlet. The gas pressure at the regulator was set at around 0.5 bar.

3 Results and discussion

Laser cutting of graphene was achieved in air and in Argon. However, under the same processing conditions, the laser ablated line width on the graphene in air was found slightly larger than that in Argon, which can be attributed to oxidative burning of graphene to volatile CO and/or CO_2 [17, 18]. Figure 3 compares the ablation line widths in air and in Ar gas. As the laser fluence increases, both the line widths increase and the line width in air is considerably wider than that in Ar.

The laser-processed regions on graphene were characterized by a 3D optical microscope (Kyence). In the optical images, the contrast between graphene-covered and graphene-free regions is high enough to identify the location of graphene. Figure 4b shows an optical microscopic photograph of a ~290 μm wide channel on graphene cut through at the laser fluence of 2.29 J/cm^2 in Argon. The dark area corresponds to the cut region. The cut edges were found to be microscopically clean. The focal point of fs laser beam was about 0.5 mm above the sample surface, which resulted in a larger spot size on the target surface. The scanning speed was 15 mm/s, which corresponds to about 20 pulses per spot.

It is noteworthy that the glass substrate beneath the graphene has little absorption at 800 nm wavelength. Since a de-focused laser beam was intentionally chosen in the ablation in Fig. 4b, the non-linear effect such as multi-photon absorption of glass was not supposed to be induced, as it is expected to occur only in a region with a high optical intensity [19]. In addition, there is no melting or ablation of the glass substrate. Thus the role of heat transfer between graphene and the substrate can be neglected in the damage of graphene.

With a lower laser fluence, narrower channels on graphene were formed. Optical image (Fig. 5a) shows precise fs-laser cutting of graphene in ambient air with defined boundaries at a laser fluence of 0.48 J/cm^2 and a scanning speed of 5 mm/s. The processing parameters resulted in 6 pulses per spot. The laser cut kerf width was measured to be about 25 μm.

To further investigate the channel characteristics as well as the lattice modifications of graphene, AFM and Raman line mapping were also performed. The AFM tapping mode 2D view of the channel in Fig. 5b clearly shows the contrast between the graphene and glass. Although the graphene single-layer thickness is only 0.33 nm in theory, the height profile reveals the thickness of graphene monolayer to be about 2 nm, which can be attributed to the adsorbates on top of the flake or in between the substrate and the flake [20, 21].

Figure 5d displays the Raman line scan spectra of the spots across the uncut area to the laser-cut zones with an increment of 1 μm (from −15 μm to −5 μm along the y axis, marked as the red line in Fig. 5c). As can be clearly seen, the uncut regions (from −15 to −11 μm) show G and 2D peaks whereas the peaks disappear in the laser-cut zones, which provides direct evidence of the complete removal of the graphene. The graphene outside the ablation site but within the laser irradiated region is also of interest. Near the laser cutting boundary ($y = -11$ μm and $y = -12$ μm), the rise in the intensity of D peak at 1350 cm^{-1} has been observed. D peak always indicates the presence of irregular edge disorder of graphene. Meanwhile, there are other effects in the evolution of the Raman spectrum: a redshift of G peak and broadening of 2D peak. According to a previous publication [22] which studied disorder in graphitic samples, the rise of D peak and FWHM broadening of all peaks suggest that the graphene undergoes the transformation into nano-crystalline graphene, instead of amorphous carbon. It is also noted in

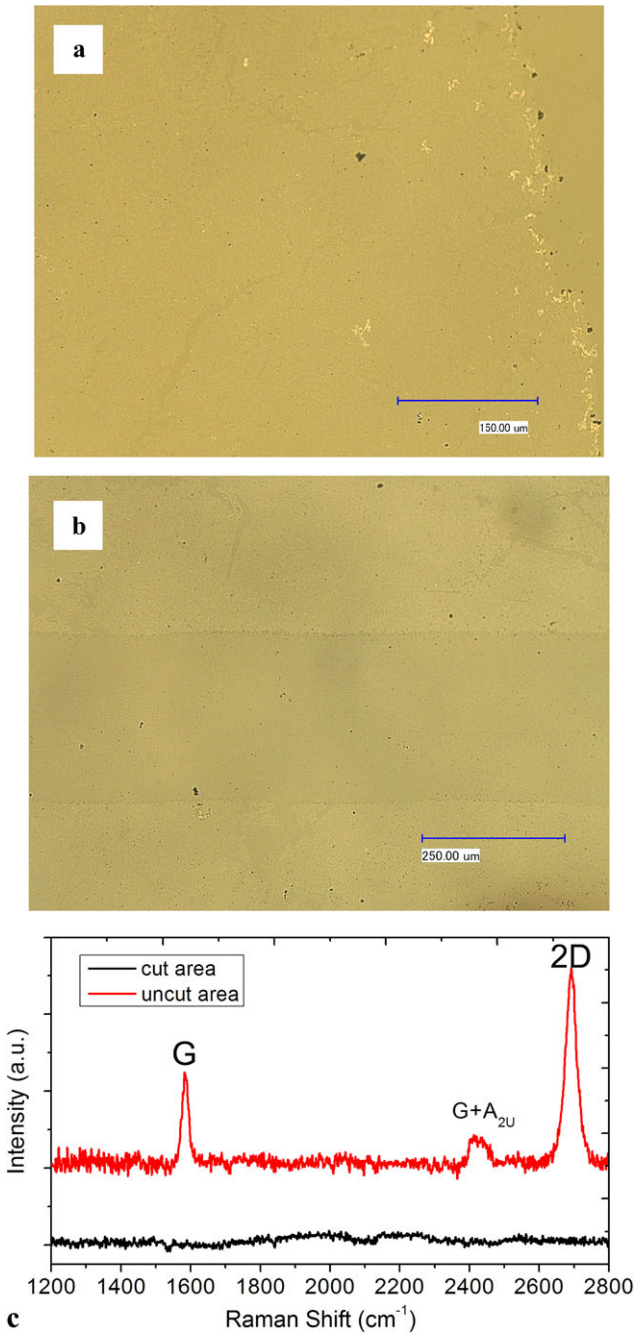

Fig. 4 Optical images of (**a**) transferred graphene sheet on glass substrate (note the border on the *right* side); (**b**) continuous channel carved on graphene in Argon by translating the sample with respect to the laser beam. (**c**) Raman spectra of the uncut (*red line*) and cut (*black line*) area

the same publication that in this regime, the intensity ratio of D peak to G peak is inversely proportional to L_a [22]:

$$\frac{I_D}{I_G} = \frac{C(\lambda)}{L_a} \tag{1}$$

where $C(\lambda)$ is a constant at a certain wavelength, and L_a is considered as an average inter-defect distance. Hence, the increase of I_D/I_G leads to a smaller nano-crystalline size L_a. On the other hand, as the sample is cut in ambient air, local oxidation of graphene takes place inevitably although the laser ablation duration is only 100 femtoseconds. Therefore, oxidized bonds may also contribute to the increase of D peak near the edge.

The observed changes of the graphene surrounding the laser-cut regions, such as an increase of D peak, broadening of 2D peak etc., indicate lattice modifications. Due to Gaussian mode intensity distribution of femtosecond laser, these modifications exist around the cut-area where the applied laser fluence is below the ablation threshold. However, despite the degradation, the graphene still survives under the laser exposure below the ablation threshold. When the laser fluence exceeds the ablation threshold, permanent damages can be formed on graphene. In Argon atmosphere, which is free of oxidative burning, the ablation threshold fluence F_{th} for single-layer graphene was determined to be 0.17 J/cm^2 at room temperature (RT), well below the ablation threshold of the glass substrate (determined to be about 3 J/cm^2), whereas the ablation of graphene in air requires a slightly lower threshold fluence of ∼0.15 J/cm^2.

Besides laser fluence, the scanning speed is also a main parameter of fs-laser processing. It is found that laser fluence has an impact on the ablation diameter or line width. Contrary to this, the ablation diameter or line width tends to be much less sensitive to the variation of scanning speed. In fact, under certain laser fluences, the decrease of scanning speed (in other words, the increase of pulse number per spot) does not necessarily increase the ablation line width, but will slightly improve the uniformity of the edges instead.

Furthermore, by reducing the hatch distance, 1∼2 μm wide, 1 mm long graphene ribbons were hatched out easily. The clean edge exhibits the unique advantage of ultra-fast laser processing. Figure 6 shows Raman microscope image of a graphene ribbon of less than 2 μm wide, and the Raman spectra of the ribbon (red line) as well as pristine graphene (black line), respectively.

A rise of D peak is noticed in the spectrum of graphene ribbon. In this case, especially when the ribbon is far smaller than the laser spot, a D peak will appear even if the sample is perfect, as the sample edges can be always seen as defects [22].

The clean patterns shown in this paper reveal the unique advantage of ultra-fast laser processing. It should be noted that the proposed technique is not limited to cutting or drilling of graphene. In fact, this technique provides a pathway for laser micro-machining of graphene. By designing the scanning path, or adjusting the laser fluence, user-defined micro-patterns with complex shapes can be easily fabricated. An example of fs laser profiling of graphene flakes on copper is shown in Fig. 7.

In order to understand the ablation mechanism, the time-dependent temperature of graphene layer under the laser ir-

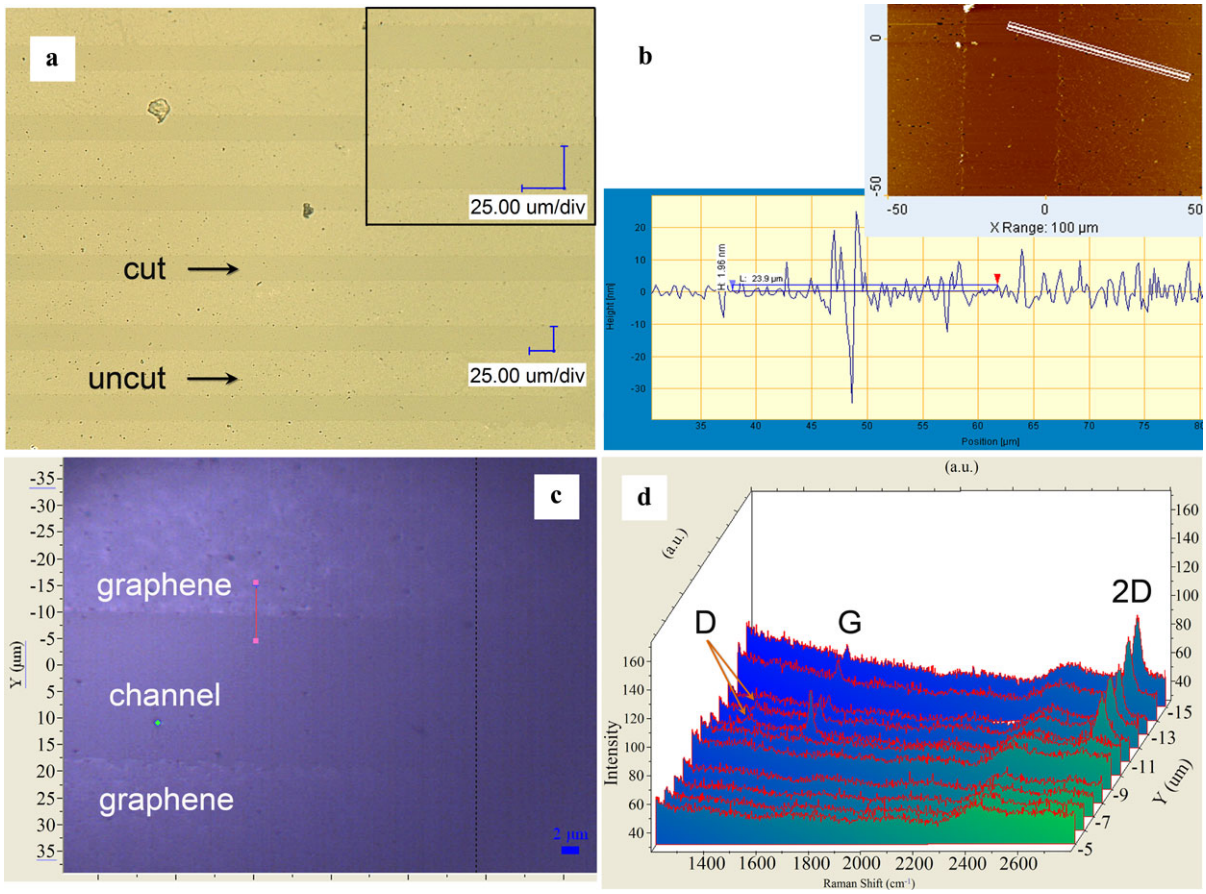

Fig. 5 (**a**) Optical image of 25 µm wide channels cut in air at 0.48 J/cm^2 laser fluence with an average spacing of 45 µm. *Inset*: enlarged view of the channels. (**b**) AFM taping mode 2D view of the same channel in (**a**). (**c**) Raman microscope image of the same pattern in (**a**). (**d**) Raman line mapping spectra across the edge [marked as the *red line* in (**c**)] of the channel

radiation was simulated using CST time domain finite difference modelling technique. The thermal conductivity and refractive index of graphene have been recently reported [5, 23], whereas the heat capacity of graphene was assumed to be close to bulk graphite in this modelling. The boundary conditions of the graphene on glass model were defined as periodic, thus a large system can be simulated by modelling a small part of it. The simulation was carried out at room temperature of 300 K.

As indicated by the calculated temperature field (Fig. 8), the femtosecond laser pulse spot centre is estimated to raise the temperature of graphene layer to above 1500 °C rapidly within 500 fs in air, and then the graphene sample takes a longer time period to cool down. The surface temperature induced by laser irradiation is high enough for graphene to react with oxygen in air, as the gasification of cleaved surface of graphite when exposed to reacting gas was reported to be 500–600 °C [24]. For laser ablation in air, the simulation results seem to indicate that the material vapourises at temperature between 1400–1500 °C which is well below the melting point of bulk graphite. The ablation temperature in Ar is similar. The high temperature physical properties of graphene are still unknown. It is expected that the boiling temperature of graphene is much lower compared with that of graphite. In addition, as the model is based on a single temperature system; some errors may be expected. For ultra-short laser pulses, the electron and lattice characteristic heating times differ greatly [25]. Thus, for a more accurate modelling to solve the problem of the coupled system for electron and lattice temperatures, a two-temperature model [26] should be introduced, which is being developed.

4 Conclusion

We have demonstrated an effective and high throughput technique for direct laser cutting and profiling of single layer graphene. The laser cutting can be achieved in air and Argon. With the help of oxygen, the cut kerf is slightly bigger in air than in Argon. By controlling the laser fluence and the scanning path, the size and shape of the pattern can be tuned easily. It is expected that this technique may not be confined

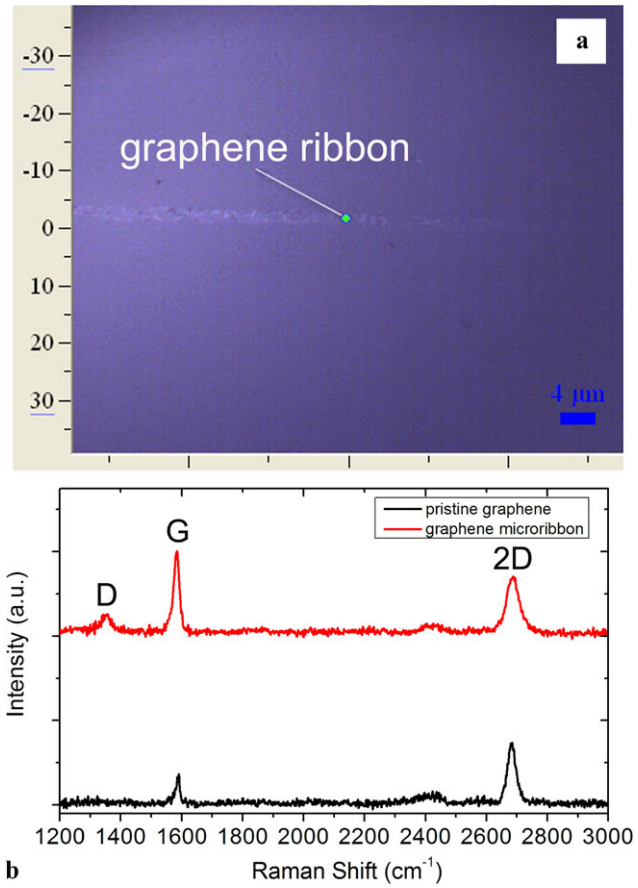

Fig. 6 (**a**) Raman microscope image of one strip of graphene ribbon. (**b**) Raman spectra of graphene ribbon and pristine graphene

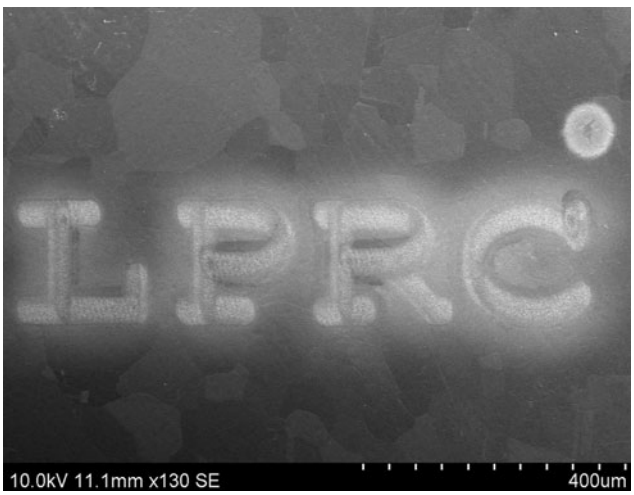

Fig. 7 SEM image of a complex micro-pattern generated on graphene coated on copper by fs laser processing

to glass substrate. This method could be extended to other substrates that have little absorption at 800 nm wavelength (e.g. SiC, often used as the substrate in graphene-based electronic devices), which implies flexibility of this approach.

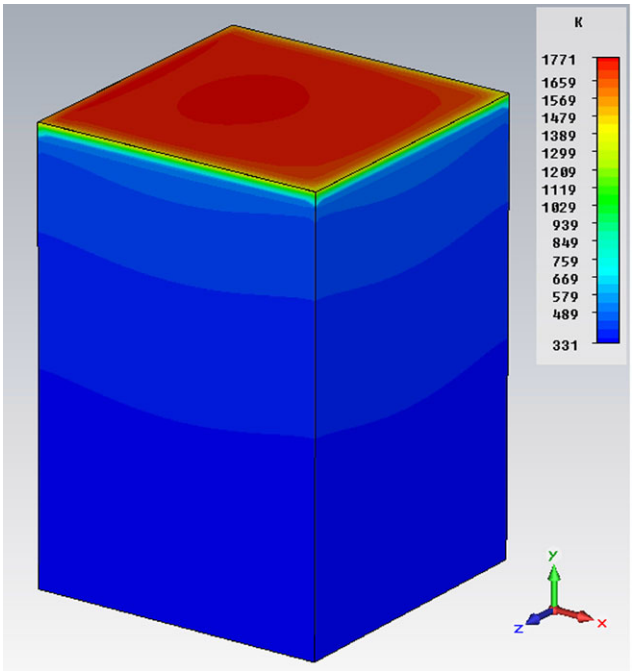

Fig. 8 Calculated temperature field of single-layer graphene film placed on top of a glass substrate, illuminated by an 800 nm fs laser

Acknowledgement The authors acknowledge the partial support of this research by Royal Academy of Engineering for multi-national collaborations through Research Exchange with China and India Award – Major Award scheme 2011–2012.

References

1. K.S. Novoselov, A.K. Geim, S.V. Morozov, D. Jiang, Y. Zhang, S.V. Dubonos, I.V. Grigorieva, A.A. Firsov, Science **306**, 666 (2004)
2. N. Papasimakis, Z. Luo, Z.X. Shen, F.D. Angelis, E.D. Fabrizio, A.E. Nikolaenko, N.I. Zheludev, Opt. Express **18**, 8353 (2010)
3. R. Dehbashi, D. Fathi, S. Mohajerzadeh, B. Forouzandeh, IEEE J. Sel. Top. Quantum Electron. **16**, 394 (2010)
4. A.K. Geim, Science **324**, 1530 (2009)
5. A.A. Balandin, S. Ghosh, W. Bao, I. Calizo, D. Teweldebrhan, F. Miao, C.N. Lau, Nano Lett. **8**, 902 (2008)
6. X.S. Li, W.W. Cai, J.H. An, S. Kim, J. Nah, D.X. Yang, R.D. Piner, A. Velamakanni, I. Jung, E. Tutuc, S.K. Banerjee, L. Colombo, R.S. Ruoff, Science **324**(5932), 1312–1314 (2009)
7. M.Y. Han, B. Ozyilmaz, Y.B. Zhang, P. Kim, Phys. Rev. Lett. **98**, 206805 (2007)
8. J. Li, R.J. Zhang, H.Q. Jiang, G.J. Cheng, Nanotechnology **22**, 475303 (2011)
9. S.W. Lee, M.F. Toney, W. Ko, J.C. Randel, H.J. Jung, K. Munakata, J. Lu, T.H. Geballe, M.R. Beasley, R. Sinclair, H.C. Manoharan, A. Salleo, ACS Nano **4**(12), 7524 (2010)
10. T. Chong, M.H. Hong, L.P. Shi, Laser Photonics Rev. **4**(1), 123–143 (2010)
11. M. Currie, J.D. Caldwell, F.J. Bezares, J. Robinson, T. Anderson, H. Chun, M. Tadjer, Appl. Phys. Lett. **99**, 211909 (2011)
12. A. Roberts, D. Cormode, C. Reynolds, T. Newhouse-Illige, B.J. LeRoy, A. Sandhu, Appl. Phys. Lett. **99**, 051912 (2011)

13. J.J. Liang, Y.S. Chen, Y.F. Xu, Z.B. Liu, L. Zhang, X. Zhao, X.L. Zhang, J.G. Tian, Y. Huang, Y.F. Ma, F.F. Li, ACS Appl. Mater. Interfaces **2**(11), 3310–3317 (2010)
14. Y.L. Zhang, L. Guo, S. Wei, Y. He, H. Xia, Q. Chen, H.B. Sun, F.S. Xiao, Nano Today **5**, 15–20 (2010)
15. L. Guo, R.Q. Shao, Y.L. Zhang, H.B. Jiang, X.B. Li, S.Y. Xie, B.B. Xu, Q.D. Chen, J.F. Song, H.B. Sun, J. Phys. Chem. C **116**, 3594 (2012)
16. A.C. Ferrari, J.C. Meyer, V. Scardaci, C. Casiraghi, M. Lazzeri, F. Mauri, S. Piscanec, D. Jiang, K.S. Novoselov, S. Roth, A.K. Geim, Phys. Rev. Lett. **97**, 187401 (2006)
17. Y. Zhou, Q. Bao, B. Varghese, L.A.L. Tang, C.K. Tan, C. Sow, K.P. Loh, Adv. Mater. **22**, 67 (2010)
18. R.S. Singh, V. Nalla, W. Chen, A.T.S. Wee, W. Ji, ACS Nano **5**(7), 5969–5975 (2011)
19. Y. Shimotsuma, K. Hirao, P.G. Kazansky, J. Qiu, Jpn. J. Appl. Phys. **44**(7A), 4735–4748 (2005)
20. B. Krauss, T. Lohmann, D.H. Chae, M. Haluska, K. von Klitzing, J.H. Smet, Phys. Rev. B **79**, 165428 (2009)
21. M. Ishigami, J.H. Chen, W.G. Cullen, M.S. Fuhrer, E.D. Williams, Nano Lett. **7**, 1643 (2007)
22. A.C. Ferrari, Solid State Commun. **143**, 47–57 (2007)
23. X. Wang, Y.P. Chen, D.D. Nolte, Opt. Express **16**(26), 22105–22112 (2008)
24. X. Chu, L.D. Schmidt, Carbon **29**, 1251 (1991)
25. S.I. Anisimov, B.S. Luk'yanchuk, Phys. Usp. **45**, 293 (2002)
26. B.S. Luk'yanchuk, S.I. Anisimov, Y.F. Lu, Proc. SPIE **4423**, 141 (2001)